NASA TECHNICAL NOTE

NASA TN D-4271

NASA TN D-4271

ENHANCEMENT OF ION CYCLOTRON WAVES IN HYDROGEN HELIUM MIXTURES

by Henry J. Hettel, Roman Krawec, George M. Prok, and Clyde C. Swett

Lewis Research Center
Cleveland, Ohio

NATIONAL AERONAUTICS AND SPACE ADMINISTRATION • WASHINGTON, D. C. • MARCH 1968

ENHANCEMENT OF ION CYCLOTRON WAVES IN HYDROGEN HELIUM MIXTURES

By Henry J. Hettel, Roman Krawec, George M. Prok, and Clyde C. Swett

Lewis Research Center
Cleveland, Ohio

NATIONAL AERONAUTICS AND SPACE ADMINISTRATION

For sale by the Clearinghouse for Federal Scientific and Technical Information
Springfield, Virginia 22151 – CFSTI price $3.00

ENHANCEMENT OF ION CYCLOTRON WAVES IN HYDROGEN HELIUM MIXTURES

by Henry J. Hettel, Roman Krawec, George M. Prok, and Clyde C. Swett

Lewis Research Center

SUMMARY

The admixture of helium to a hydrogen plasma atmosphere has increased the radio-frequency power absorption in the ion-cyclotron mode. Measurements of power absorption, plasma radius, electron density, and magnetic flux density at the peak power point were obtained as a function of plasma composition. A relation was derived involving these experimental parameters and the ion density. It is shown that the observed power enhancement can be explained if it is assumed that the metastable states of the helium atoms react with hydrogen atoms and molecules to increase the plasma ion density.

INTRODUCTION

For efficiency in heating protons by means of an ion-cyclotron wave, the proton density should be on the order of 10^{18} per cubic meter (refs. 1 to 4). The power which can be coupled into the wave is dependent not only on the ion density, but also on the effective proton plasma radius. Thus, for a given experimental configuration, increased power can be coupled into the wave if a way can be found to increase the plasma radius and/or the ion density (provided the ion density does not already exceed the optimum).

On theoretical grounds, the admixture of helium to the hydrogen support gas promised to provide such a means via collisions of the second kind between hydrogen species and metastable helium atoms. The 19.8 electron volts (3.17 aJ) of the helium 2^3S_1 metastable state is sufficient to ionize hydrogen atoms and dissociate hydrogen molecules. Thus, the helium metastables produced by electron impact in the primary electron beam region (refs. 5 and 6), can diffuse across the confining magnetic-field lines and produce ionization beyond the confines of the primary beam, thereby increasing the proton plasma radius. Simultaneously, an increase in proton density will result,

the degree of increase depending on the magnitude of the proton production rate ascribable to helium metastables relative to that ascribable to electron impact. A series of measurements were made in the ion cyclotron resonance apparatus (ref. 5) using various mixtures of hydrogen and helium gas. Variations were observed not only in the power absorbed, but also in plasma radius, electron density, and resonance frequency as the gas composition was changed. A theoretical model is set forth whereby the role of the metastable helium atom in increasing the proton density may be deduced.

APPARATUS

A schematic diagram of the experimental apparatus (ref. 5) is shown in figure 1.

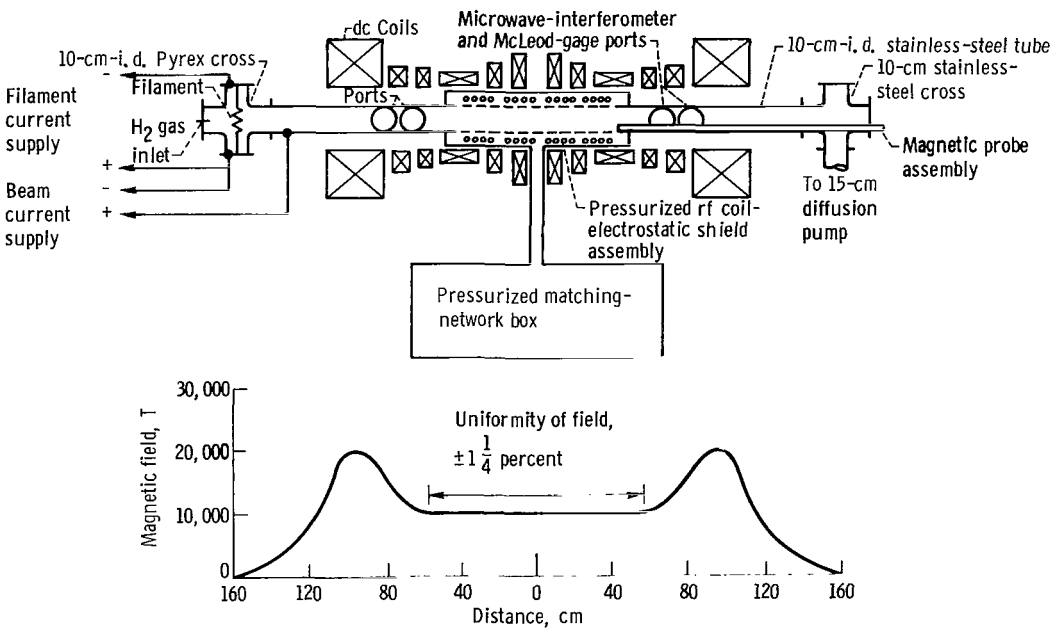

Figure 1. - Configuration of ion-cyclotron resonance apparatus 2B (ICRA 2B).

The vacuum chamber is a 2.7-meter-long by 10-centimeter-diameter tube consisting of an 84-centimeter-long aluminum oxide center section with stainless-steel end sections. The axial magnetic field has a 2 to 1 mirror ratio, can operate continuously, and may be varied in strength to 1 tesla (10 000 G) in the flat-field portion between the mirrors. The magnetic-field strength at the cathode location is about 15 percent of the flat-field value.

A commercial grade of hydrogen gas or a previously prepared and analyzed mixture of commercial grade hydrogen and commercial grade helium was fed into one end of the vacuum chamber and pumped out the other end. The flow rate, and thus the pressure,

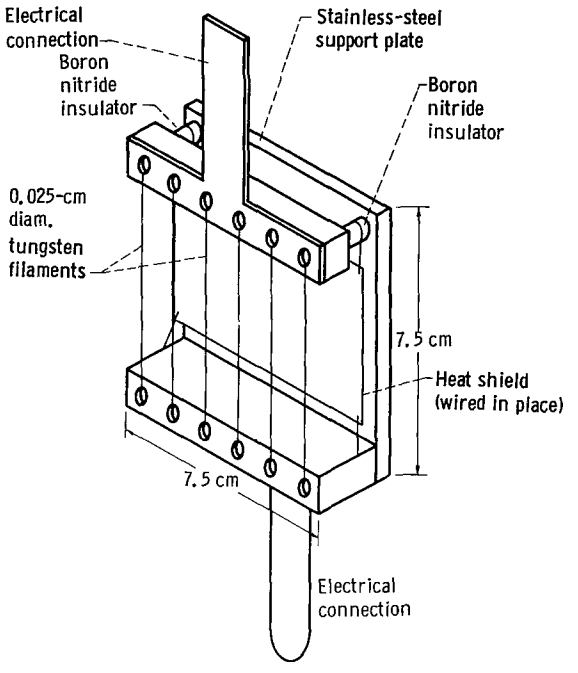

Figure 2. - Plane filament support.

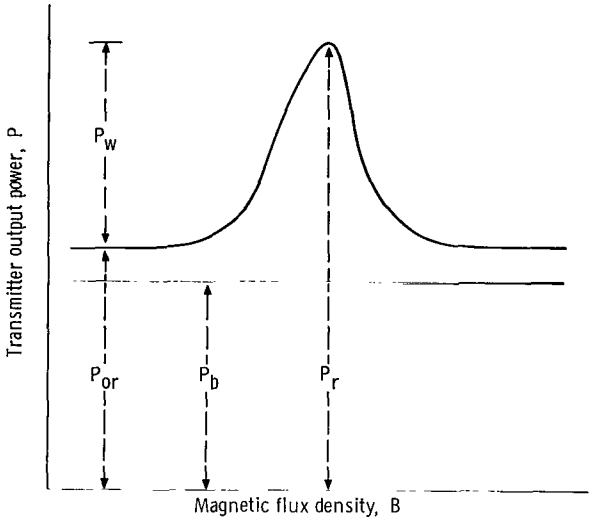

Figure 3. - Schematic plasma power curve.

was regulated by means of a variable leak valve upstream of the vacuum chamber. The pressure was measured by means of a McLeod gage mounted about 0.9 meter downstream of the center of the test chamber, which is about 2.7 meters from the hydrogen inlet. Under these conditions, there was a twofold pressure drop from one end of the test section to the other. For all experiments reported herein, the pressure of the test gas was held constant at 2.00±0.05 microns (0.267±0.007 N/m^2) as measured by the McLeod gage.

A sketch of the hot cathode electron source used is presented in figure 2. Details of construction and operation have been previously published (ref. 6).

THEORY

Wave Power Input Related to Experimental Parameters

A schematic plot of radio-frequency (RF) power input to the plasma with variation in magnetic-flux density is shown in figure 3, where P_r is the transmitter output power at resonance and P_{or} is the off-resonance or no-wave-propagation power, so that their difference P_w is the power being fed into the ion cyclotron wave. The base power P_b is the power dissipated in the electrical components when there is no plasma. It is

measured by running the apparatus in the same fashion as for a normal test run, except that no support gas is admitted to the test chamber so that no plasma can exist.

We shall be concerned primarily with the peak power point. According to Stix (ref. 7), the quantity P_w/P_b (defined by him as W) is given by

$$\frac{P_w}{P_b} = QUV \tag{1}$$

where Q is the usual figure of merit for a coil (the ratio of its inductive reactance to its resistance) and U and V are defined as follows:

$$U = \frac{8\ell R^2\Omega^2}{\pi\lambda^3\left(M - \frac{1}{4}\right)^4} \tag{2}$$

$$V = \frac{I_1(kR)K_1(kR_c)}{I_1(kR_c)K_1(kR)} L_{fs} \tag{3}$$

The notation used in these and subsequent relations are defined in appendix A. The approximate dispersion relation for ion-cyclotron waves is given by Stix (ref. 7, eqs. 10 and 26) as

$$\Omega^2 = \left(1 + \frac{Z^2 n\lambda^2}{2.03\times10^{18}A}\right)^{-1} \tag{4}$$

Inserting the values of U and V given by equations (2) and (3) yields for equation (1)

$$\frac{P_w}{P_b} = \frac{8Q\ell R^2\Omega^2 L_{fs}}{\pi\lambda^3\left(M - \frac{1}{4}\right)^4} \frac{I_1(kR)}{K_1(kR)} \frac{K_1(kR_c)}{I_1(kR_c)} \tag{5}$$

The gross behavior of the Bessel function ratio I_1/K_1 may be extracted by writing them as the product of a deviation term δ and their small argument approximations

$$I_1(\xi) = \frac{\xi}{2}, \quad K_1(\xi) = \frac{1}{\xi} \tag{6}$$

for $\xi < 1$. Thus, $\delta(kR)$ is defined by the relation

$$\frac{I_1(kR)}{K_1(kR)} = \frac{k^2R^2}{2}\,\delta(kR) \tag{7}$$

which, on noting that $k = 2\pi/\lambda$, yields for equation (5)

$$\frac{P_w}{P_b} = \frac{8Q\ell\, L_{fs}}{\pi\left(M - \frac{1}{4}\right)^4 R_c^2}\,\frac{\delta(kR)}{\delta(kR_c)}\,\frac{R^4\Omega^2}{\lambda^3} \tag{8}$$

In arriving at equation (2), Stix specified that the wavelength in the plasma was equal to the geometrical coil wavelength. A more exact specification might be that the plasma wavelength be equal, not to the geometrical coil wavelength, but rather to the apparent coil wavelength as seen by the plasma. For a perfectly wound infinite-length coil, the geometrical and apparent coil wavelengths are the same, but, for a finite length coil with end effects, the two may differ. Indeed, a Fourier decomposition of the RF vacuum magnetic field under our coil shows significant contributions from wavelength components of 89, 44.5, and 29.6 centimeters (ref. 5). Thus, we have no a priori knowledge even of the gross magnitude of the plasma wavelength, let alone of what small changes in apparent coil wavelength such coil loading factors as proton density level and radial density profile may engender.

Our ignorance of the apparent coil wavelength may be obviated by letting the plasma tell us what is the coil wavelength it sees. This is readily done by use of the dispersion relation. Thus, if equation (4) is written for the proton-cyclotron wave by setting $Z = A = 1$, then

$$\frac{1}{\lambda^3} = \frac{n^{3/2}\Omega^3}{(1 - \Omega^2)^{3/2}(2.03\times10^{18})^{3/2}} \tag{9}$$

which yields, upon substitution into equation (8),

$$\frac{P_w}{P_b} = \frac{8Q\ell\, L_{fs}}{2.83\times10^{27}\pi\left(M - \frac{1}{4}\right)^4 R_c^2}\,\frac{\delta(kR)}{\delta(kR_c)}\,\frac{n^{3/2}R^4\Omega^5}{(1 - \Omega^2)^{3/2}} \tag{10}$$

Grouping the constants permits the writing of

$$\frac{P_w}{P_b} = C \frac{n^{3/2} R^4 \Omega^5}{(1 - \Omega^2)^{3/2}} \frac{\delta(kR)}{\delta(kR_c)} \tag{11}$$

from which it is seen that, in view of the low order dependence of Ω on n, indicated by equation (4), an increase in the value of n and/or R by helium admixture should increase the power coupled into the plasma wave.

For a helium-hydrogen mixture whose composition is given by x, the mole fraction helium, the quantity $(P_w/P_b)_x$ may be conveniently compared to the similar quantity for a pure hydrogen plasma (x = 0) by defining a ratio F such that

$$F \equiv \frac{(P_w/P_b)_x}{(P_w/P_b)_0} = \frac{(P_w)_x}{(P_w)_0} \tag{12}$$

The base power P_b is measured under no-gas conditions, and it is independent of x. Thus, F is simply the wave power ratio between the mixture and pure hydrogen.

If coupling is negligible between the proton-cyclotron wave and the He^+ cyclotron wave, then equations (1) to (11) may be written not only for pure hydrogen supporting atmospheres, but also for hydrogen-helium mixtures as well. Hence, in view of equation (11), equation (12) becomes

$$F = \left(\frac{n_x}{n_0}\right)^{3/2} \left(\frac{R_x}{R_0}\right)^4 \left(\frac{\Omega_x}{\Omega_0}\right)^5 \left(\frac{1 - \Omega_0^2}{1 - \Omega_x^2}\right)^{3/2} \left(\frac{\delta(k_x R_x)/\delta(k_x R_c)}{\delta(k_0 R_0)/\delta(k_0 R_c)}\right) \tag{13}$$

It will prove convenient to define a quantity Δ by

$$\Delta \equiv \frac{\delta(k_x R_x)/\delta(k_x R_c)}{\delta(k_0 R_0)/\delta(k_0 R_c)} \tag{14}$$

For x = 0, Δ is unity. As a first order approximation, take it to be unity for all other x as well. The validity of this approximation is demonstrated in appendix B, wherein it is shown to have no significant effect on the results of this investigation. Thus, equation (13) becomes

$$F_{meta} = \left(\frac{n_x}{n_0}\right)^{3/2} \left(\frac{R_x}{R_0}\right)^4 \left(\frac{\Omega_x}{\Omega_0}\right)^5 \left(\frac{1 - \Omega_0^2}{1 - \Omega_x^2}\right)^{3/2} \tag{15}$$

Experimental measurements are acquirable for the quantities R_x/R_0, Ω_x, and Ω_0, so that prediction of F depends only on the prediction of n_x/n_0. The functional x-dependence of n_x/n_0 is derived on the basis of enhanced hydrogen ionization by helium metastables. Insertion of the result into equation (15), together with the experimental values of Ω and R_x/R_0, will provide F_{met} as a function of x. The correctness of the metastable interaction assumption may then be assessed by comparing F_{met} with F_{exp}.

Proton Density and Helium Metastables

In evaluating the effect of the helium metastables on the proton production and loss rates, one must use a model consistent with the known characteristics of the plasma being studied. The plasma of this experiment has a total neutral density of about 5×10^{19} per cubic meter. From electron density measurements the degree of ionization is in the vicinity of 0.5 percent, and the degree of dissociation is estimated from visual spectroscopic observations to be between 5 and 25 percent. The mean free path of the molecular species is about 20 centimeters, whereas the discharge tube radius is 5 centimeters. Thus the following assumptions are consistent with the plasma of this experiment:

(1) Collisions between electrons and ionized species are insignificant because of their low concentrations with respect to those of hydrogen and helium.

(2) Wall losses of ions and excited plasma neutrals predominate over losses through plasma-phase reactions; hence, loss rates of ions and metastable atoms will be directly proportional to their respective concentrations. Thus, the reactions occurring in the plasma are restricted to those shown in table I and have the rate constants defined therein. A discussion of why these reactions were chosen is presented in appendix C.

TABLE I. - PLASMA REACTIONS

Production reaction	Cross section	Loss reactions	Rate constant
$H_2 \xrightarrow{e^*} 2H$	σ_1	$H^+ \xrightarrow[wall]{+e} 1/2\ H_2$	K_1
$H_2 + He^m \rightarrow 2H + He^o$	σ_2	$H \xrightarrow[wall]{} 1/2\ H_2$	K_2
$H \xrightarrow{e^*} H^+ + e$	σ_3	$He^m \xrightarrow[wall]{} He^o$	K_3
$H + He^m \rightarrow H^+ + e + He^o$	σ_4	----------	---
$He \xrightarrow{e^*} He^m$	σ_5	----------	---

The duration of plasma operation being on the order of minutes, a steady state is assumed, permitting rate balance equations to be written for all species. For the gas phase reaction

$$A + B \rightarrow X + Y \tag{16}$$

The production rate per unit volume, may be written

$$\frac{dn(X)}{dt} = \frac{dn(Y)}{dt} = n(A)\, n(B)\sigma_{AB}v_{AB} \tag{17}$$

where $n(A)$ and $n(B)$ are the number densities of the reactants A and B, σ_{AB} is the cross section for the reaction in question, and v_{AB} is the velocity of closure of A and B. As written, equation (17) ignores the fact that σ_{AB} is a function of v_{AB}, and that, for an assembly of particles, the average value of the product $\sigma_{AB}v_{AB}$ should be used. For electron impact reactions, σ_{AB} varies as log v_{AB}. Anticipating that v_{AB} will be found to vary only a little, so that σ_{AB} will vary even less, we shall consider all σ_{AB}'s to be constants. Under these circumstances, v_{AB} then becomes the average value of the electron velocity distribution.

The total plasma production rate for any species is given by the product of the plasma volume and the production rate per unit volume. Thus, for a uniform plasma of radius R and length l

$$\frac{dN(x)}{dt} = n(A)n(B)\sigma_{AB}v_{AB}\pi R^2 l \tag{17a}$$

where $dN(x)/dt$ is the total plasma production rate. If the plasma losses are to be all to the wall, then all species formed in the plasma must pass through the plasma boundary. Thus, the total plasma loss rate is the product of the plasma surface area and the loss rate per unit plasma surface area. Thus,

$$-\frac{dN(x)}{dt} = K(x)n(x)2\pi R l \tag{17b}$$

where $K(x)$ is the loss rate constant of species x.

For the reactions of table I, equating the proton production and loss rates yields

$$\left|\frac{dN(H^+)}{dt}\right| = n_e n(H)\sigma_3 v + n(H)n(He^m)\sigma_4 w = 2K_1 n(H^+)/R \tag{18}$$

where v is the average closure velocity of electrons with plasma neutrals, and w is correspondingly the average closure velocity between plasma neutrals. Similarly, for the helium metastables,

$$\left|\frac{dN(He^m)}{dt}\right| = n_e n(He)\sigma_5 v = 2K_3 n(He^m)/R \tag{19}$$

Elimination of $n(He^m)$ between equations (18) and (19) yields

$$n(H^+) = Rn_e n(H)\left\{\frac{\sigma_3 v}{2K_1} + \frac{\sigma_4 w \sigma_5 v R}{4K_1 K_3} n(He)\right\} \tag{20}$$

A relation exists between $n(H)$ and $n(He)$ which stems from the composition of the gas feeding the plasma. This relation may be expressed as follows: The total number density $n(tot)$ of all constituents in the feed gas is given by

$$n(tot)^0 = n(H_2)^0 + n(He)^0 \tag{22}$$

where the superscript zeros denote feed gas to distinguish them from the corresponding quantities in the plasma which carry no superscript. In terms of the mole fraction helium x

$$n(He)^0 = xn(tot)^0 \tag{23a}$$

$$n(H_2)^0 = (1 - x)n(tot)^0 \tag{23b}$$

Furthermore, a quantity m, the degree of dissociation, may be defined as that fraction of the original molecular hydrogen in the mixture that has dissociated into atoms. Thus, since every hydrogen molecule yields two atoms on dissociation,

$$n(H) = 2mn(H_2)^0 = 2m(1 - x)n(tot)^0 \tag{24a}$$

and

$$n(H_2) = (1 - m)n(H_2)^0 = (1 - m)(1 - x)n(tot)^0 \tag{24b}$$

Having now obtained expressions for the plasma quantities $n(H)$ and $n(H_2)$, it remains only to express $n(He)$. Since the loss of ground-state helium atoms due to ionization, metastable formation, etc., is insignificant in the slightly ionized plasma of this

experiment, the helium density in the plasma is different from the helium density in the feed gas only because of the slight amount of neutral heating which occurs in the plasma. The temperature rise of the plasma neutrals is estimated to be about 50° C. Thus,

$$n(He) = tn(He)^0 \tag{25}$$

where the factor t takes care of the reduction in plasma helium density resulting from thermal expansion of the plasma atmosphere. Equation (23a) then becomes

$$n(He) = xtn(tot)^0 \tag{26}$$

Now that the relations between n(H), $n(H_2)$, and n(He) resulting from feed gas composition are established, they may now be inserted into equation (20) yielding, after factoring the quantity $\sigma_3 v/2K_1$,

$$n(H^+) = \frac{\sigma_3 n(tot)^0}{K_1} Rvm(1 - x)n_e \left[1 + \frac{\sigma_4 \sigma_5 n(tot)^0 wt}{2\sigma_3 K_3} xR\right] \tag{27}$$

Of the quantities in equation (27), v, m, and n_e vary significantly with x. The remaining quantities σ_j, K_j, w, and t are, at best, second order in x, a fortunate happenstance because there is no experimental data on the variation of these with x. Thus, the following constants are defined as

$$\alpha \equiv \frac{\sigma_3 n(tot)^0}{K_1} \tag{28a}$$

$$\gamma \equiv \frac{\sigma_4 \sigma_5 n(tot)^0 wtR_0}{2\sigma_3 K_3} \tag{28b}$$

with the aid of which equation (27) becomes

$$n_x(H^+) = \alpha v_x m_x (1 - x) n_{ex} R_x \left(1 + \gamma \frac{R_x}{R_0} x\right) \tag{29}$$

in which the x-dependence of the pertinent quantities has been indicated by subscripting. For a pure hydrogen plasma, for which x = 0, equation (29) becomes

$$n_0(H^+) = \alpha v_0 m_0 n_{e0} R_0 \tag{30}$$

Thus, from equations (29) and (30), the ratio n_x/n_0 is

$$\frac{n_x(H^+)}{n_0(H^+)} = \frac{v_x}{v_0}\frac{m_x}{m_0}\frac{n_{ex}}{n_{e0}}(1 - x)\frac{R_x}{R_0}\left(1 + \gamma x\frac{R_x}{R_0}\right) \tag{31}$$

An expression for m_x/m_0 is readily derived by considering the probable dissociation reactions in the plasma, as discussed in appendix C. The rate balance equations for the atomic hydrogen production and loss reactions of table I yield the following relation:

$$\left|\frac{dN(H)}{dt}\right| = 2\sigma_1 v n_e n(H_2) + 2\sigma_2 w n(H_2) n(He^m) = 2K_2 n(H)/R \tag{32}$$

After rearrangement of equation (32) and use of equation (19) to eliminate $n(He^m)$,

$$n(H) = 2Rn_e n(H_2)\left[\frac{\sigma_1 v}{2K_2} + \frac{\sigma_2 w \sigma_5 v R}{4K_2 K_3}\, n(He)\right] \tag{33}$$

When equations (24a), (24b), and (26) are used, equation (33) becomes

$$\frac{m}{1 - m} = \frac{\sigma_1 v}{2K_2} n_e\left[1 + \frac{\sigma_2\sigma_5 w n(tot)^0}{2\sigma_1 K_3} xR\right] \tag{34}$$

The coefficient of x may be expressed in terms of γ, defined by equation (28b) by writing

$$\frac{\sigma_2\sigma_5 w n(tot)^0 R_0}{2\sigma_1 K_3} = \left(\frac{\sigma_2}{\sigma_1}\frac{\sigma_3}{\sigma_4}\right)\left[\frac{\sigma_4\sigma_5 w n(tot)^0 R_0}{2\sigma_3 K_3}\right] = \frac{\sigma_2}{\sigma_1}\frac{\sigma_3}{\sigma_4}\gamma \tag{35}$$

Thus, by defining the quantities

$$\beta = \frac{\sigma_2}{\sigma_1}\frac{\sigma_3}{\sigma_4} \tag{36a}$$

$$\xi = \frac{\sigma_1}{2K_2} \tag{36b}$$

and using x-subscripts to designate the x-dependent parameters, equation (34) may be written as

$$\frac{m_x}{1 - m_x} = \xi v_x n_{ex} R_x \left(1 + \beta\gamma x \frac{R_x}{R_0}\right) \tag{37}$$

Writing equation (37) for the pure hydrogen case yields

$$\frac{m_0}{1 - m_0} = \xi v_0 n e_0 R_0 \tag{38}$$

whereupon the ratio of equations (37) and (38) is

$$\left(\frac{m_x}{m_0}\right)\left(\frac{1 - m_0}{1 - m_x}\right) = \frac{v_x}{v_0} \frac{n_{ex}}{n_{e0}} \frac{R_x}{R_0} \left(1 + \beta\gamma x \frac{R_x}{R_0}\right) \tag{39}$$

Thus, on substitution of equation (31) into equation (15), F_{met} is given by

$$F_{met} = \left(\frac{R_x}{R_0}\right)^{11/2} \left(\frac{\Omega_x}{\Omega_0}\right)^5 \left[\left(\frac{1 - \Omega_0^2}{1 - \Omega_x^2}\right)\left(\frac{v_x}{v_0}\right)\left(\frac{m_x}{m_0}\right)\left(\frac{n_{ex}}{n_{e0}}\right) (1 - x) \left(1 + \frac{R_x}{R_0} \gamma x\right)\right]^{3/2} \tag{40}$$

with m_x/m_0 being given by equation (39).

EXPERIMENTAL RESULTS

Wave Power Measurements

A composite plot of total input power against magnetic flux density in the vicinity of the peak power point is presented in figure 4 for hydrogen and the six mixtures studied. Gas composition is indicated by x, the mole fraction of helium in the mixture.

No variation in plasma power input with magnetic flux density was observed for the pure helium plasma $x = 1$ over the 0.3 to 0.5 tesla range studied. This justifies the assignment of the plasma power input at 0.32 tesla[1] in the mixture under study as

[1]No significance should be attached to the specific P_{or} value at 0.32 tesla, since the P_{or} is constant over the range from 0.30 to 0.36 tesla. The 0.32-tesla value happened to be convenient to establish in our device.

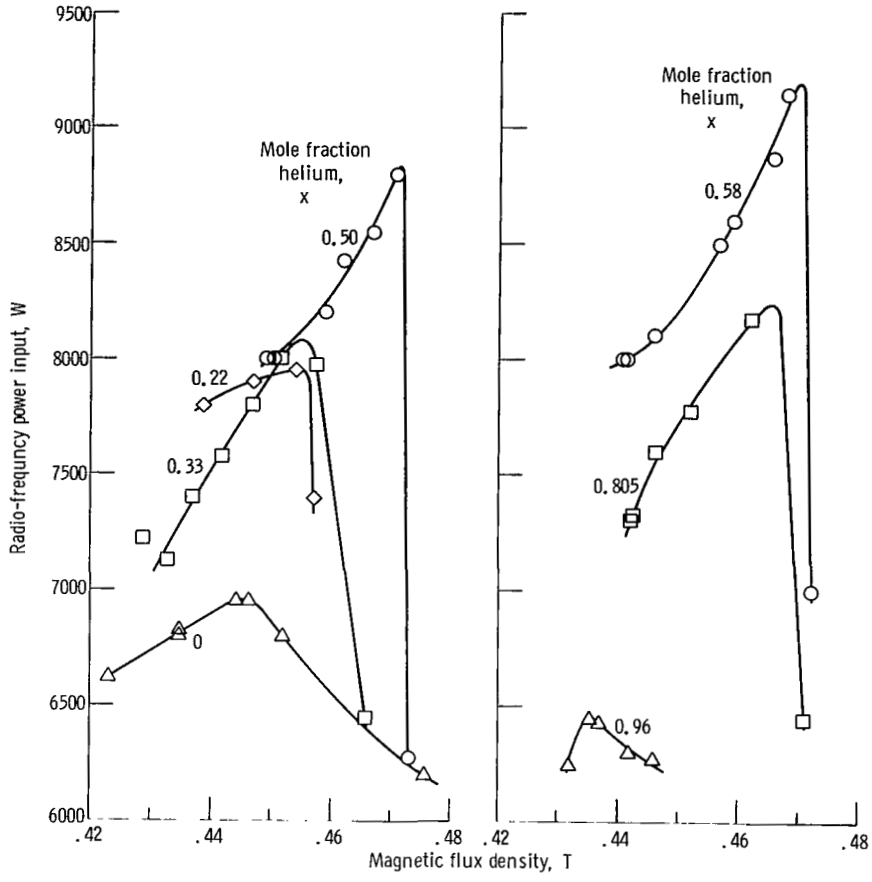

Figure 4. - Experimental plasma power curves.

being also the off-resonant power input P_{or} at the peak power field for that mixture. Thus, the wave power input at any flux density B is given by the difference between the total-power input at that flux density P(B) and the total power input at 0.32 tesla P(0.32); that is,

$$P_w(B) = P(B) - P(0.32) \tag{41}$$

Hence, for B = B (peak) of each mixture

$$P_w = P_r - P(0.32) \tag{42}$$

For pure hydrogen, P_w was 950 watts.

The quantity F_{exp}, defined by equation (12), is plotted against gas composition in figure 5. The enhancement of wave power input by helium admixture is seen to peak near x= 0.6.

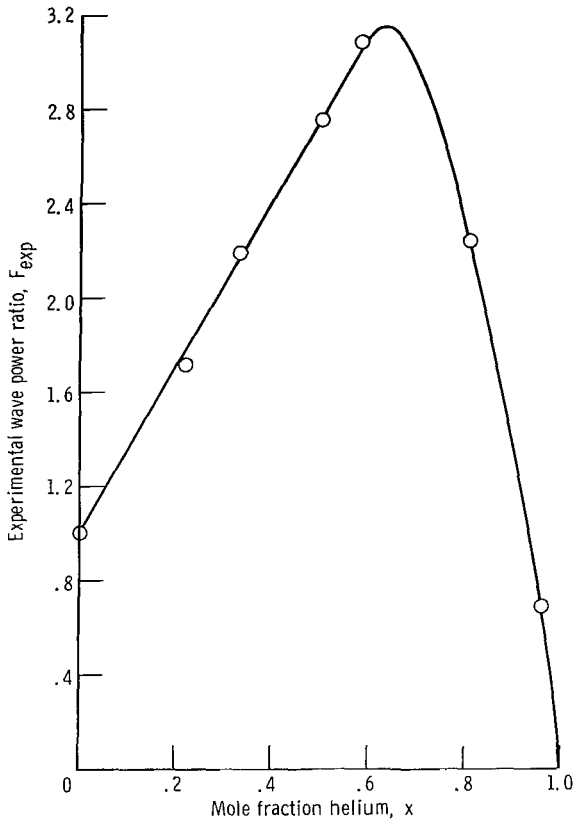

Figure 5. - Experimental wave power function.

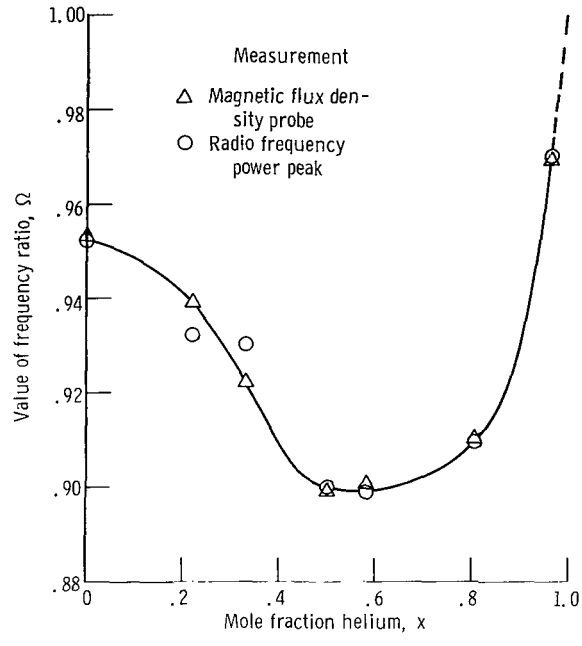

Figure 6. - Experimental values of frequency ratio.

Measurement of Coil Driving Frequency to Ion Cyclotron Frequency Ratio

The quantity Ω is defined by Stix (ref. 7) as the ratio of the angular frequency of the propagated wave to the angular ion-cyclotron frequency, the latter being given by ZeB/m_p. For the experimental case where the driving frequency ω is fixed, Ω becomes the ratio B_{ci}/B, where $B_{ci} = \omega m_p / Ze$ and B is the magnetic flux density at which maximum power transfer to the wave occurs. The values of Ω so obtained are plotted against x in figure 6.

Another, and independent, measurement of Ω was also made, however. A magnetic probe sensitive to the axial component of the plasma wave was positioned downstream of the RF coil. The construction, operation, and positioning of this probe is described in reference 5. The amplitude of the signal from this probe is a measure of the strength of the wave passing through the plasma, and hence the peak probe amplitude is also an indicator of Ω. The values of Ω obtained from the probe measurements are also plotted in figure 6.

Except for the $x = 0.22$ and $x = 0.328$ points, the agreement between the two

measurements of Ω is good. Since we believe that the probe is a more reliable indicator of Ω than the power measurements, we shall in all cases use the probe values in the calculations.

Plasma Radius Measurements

The radial distribution of the radiation emitted by the plasma was obtained by the standard technique of performing an Abel inversion on the measured chord intensity distribution (ref. 8). The device for obtaining the measured chord intensity distribution (fig. 7) is basically a two-slit collimator with the slits parallel to the plasma axis. The cross-sectional dimensions of the plasma slab viewed are 0.75 by 10 millimeters. Since no dispersing element was interjected between the photocathode and the collimator of the scanner and since the viewing port window was fused quartz, the photomultiplier saw all radiation within the envelope of its spectral sensitivity curve.

A plot of the radial intensity distribution of the plasma is shown in figure 8 for the peak power point of the $x = 0.50$ mixture. This distribution is typical of all those observed in this study. The significance of the intensity distribution is that, in a tenuous and slightly ionized plasma such as ours, the radiant intensity emitted from a point is directly proportional to the electron density at that point.

Two problems exist in interpreting the radial distribution curves: (1) The quantity of interest is the effective proton plasma radius, whereas the quantity measured is the radial distribution of electrons possessing sufficient energy to excite hydrogen molecules and helium atoms, and (2) the radial distribution is a smooth function for which the designation of a single value characterizing an effective radius is not free of ambiguity. With respect to the first problem, the assumption will be made that the effective proton plasma radius is directly proportional to the effective electron plasma radius since, after all, the ions are generated by ionization of neutrals by the same energetic plasma electrons that are responsible for the excitation of the neutrals. With respect to the second problem, the intensity-weighted average radius of the distribution $\bar{R}$, given by

$$\bar{R} = \frac{\int_0^\infty I(r) r \, dr}{\int_0^\infty I(r) \, dr} \tag{43}$$

is used as the characteristic radius of the plasma. The quantity $I(r)$ is, of course, the radial intensity distribution of the plasma as derived from the Abel inversion of the chord intensity distribution.

The quantity to be inserted into equation (15) is the proton plasma radius ratio

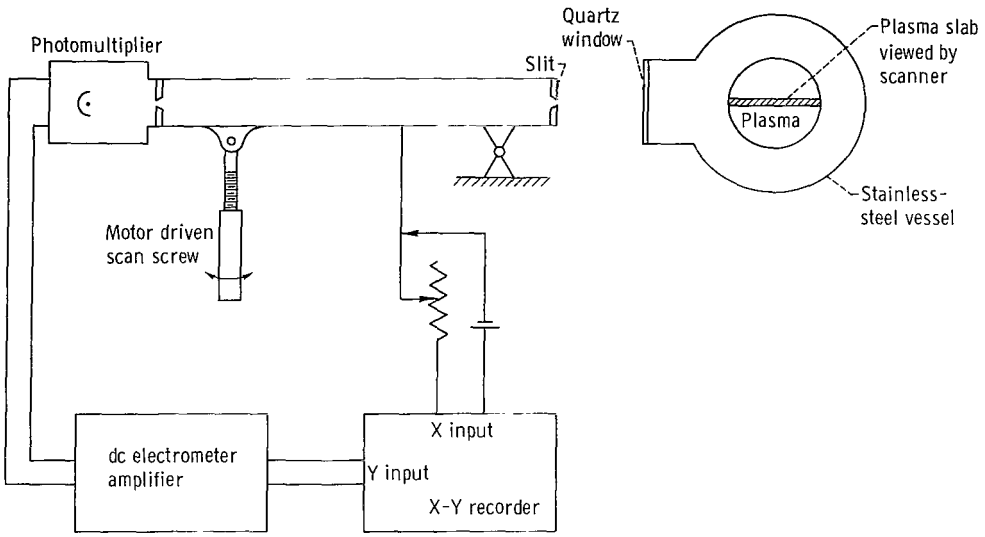

Figure 7. - Schematic diagram of radiation scanner.

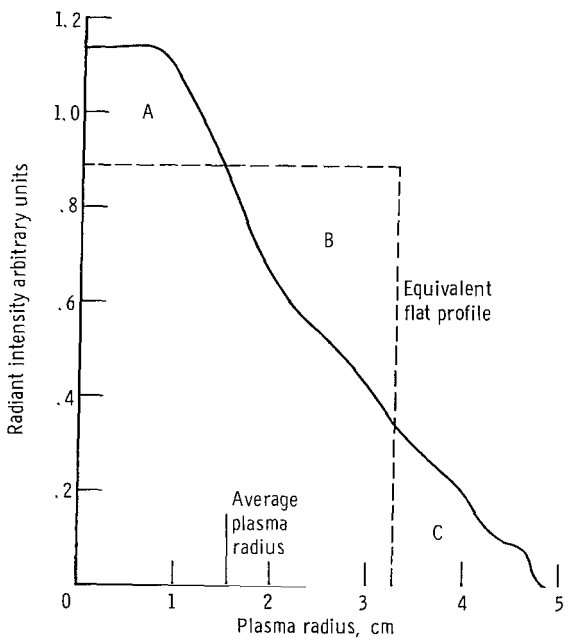

Figure 8. - Typical experimental radial intensity distribution.

R_x/R_0. If $\bar{R}$ is proportional to the effective electron plasma radius, and if this, in turn, is proportional to the proton plasma radius, then the error in R_x/R_0 will be less than the error in the absolute value of the effective plasma radius. To illustrate this, two other methods of obtaining a characteristic radius were investigated: (1) The calculation of $\bar{R^2}$ in the standard manner analogous to equation (43), and (2) the calculation of an equivalent flat profile (dashed line in fig. 8) such that area A equals area C equals one-half area B. Although the magnitude of the three characteristic radii differed greatly for a given radial distribution, curves of R_x/R_0 calculated from each technique were coincident with one another to within a few percent.

A plot of R_x/R_0 at the peak power point, derived from the R values is presented in figure 9.

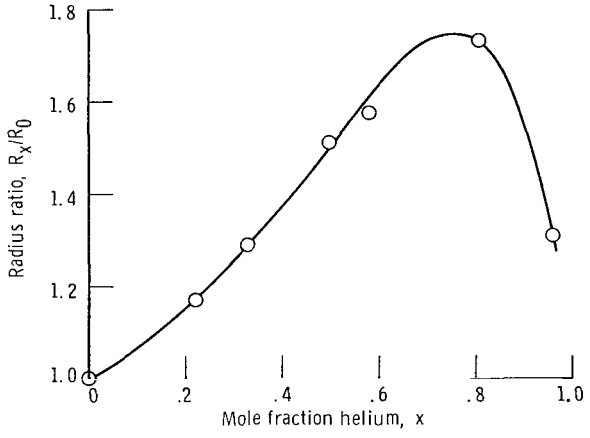

Figure 9. - Experimental radius ratios.

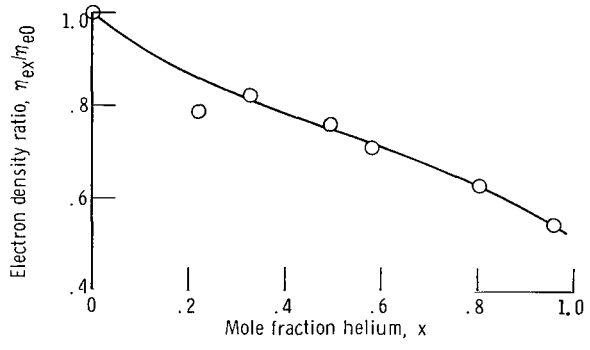

Figure 10. - Experimental electron density ratios.

Electron Density Measurements

An 8-millimeter microwave interferometer was used to measure space average values of the electron density. Complete details of the system and its operation are given in reference 6. The plot of the electron density ratio at the peak power point is given as a function of gas composition in figure 10.

Electron Velocity Measurements

The total potential drop required to sustain a 15-ampere beam current was another of the experimental parameters measured. It was shown in reference 6 that the electron energy in the primary beam was directly proportional to the beam power input. Thus, since the current was held constant for all runs, the electron energy is proportional to the measured potential drop. It follows that

$$\frac{v_x}{v_0} = \left(\frac{E_x}{E_0}\right)^{1/2} \tag{44}$$

where E_x is the potential drop across the plasma whose composition is characterized by its mole fraction x. The electron velocity ratio at the peak power point is given as a function of gas composition in figure 11.

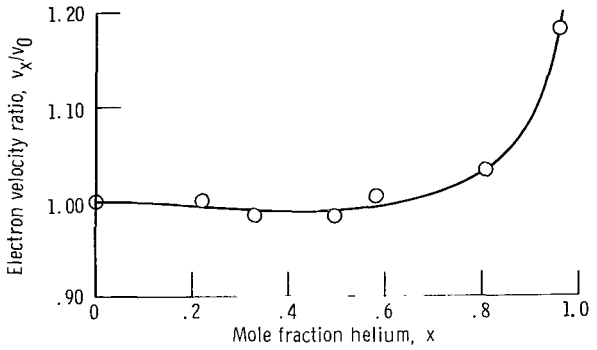

Figure 11. - Experimental electron velocity ratios.

DISCUSSION

Equations (39) and (40) can, in principle, be used to calculate F_{met} for each of the gas mixtures studied. Experimental values are available for Ω_x, Ω_0, and the ratios R_x/R_0, n_{ex}/n_{e0}, and v_x/v_0. Thus, if m_0, β, and γ were known, m_x could be calculated from equation (39) and then F_{met} obtained from equation (40).

Since m_0, the degree of dissociation of the pure hydrogen plasma, is not known, the range of its probable value must be determined. By definition m_0 is a number between zero and unity. The best estimate for its value in the plasma of this experiment is 0.15, so its probable range is between 0 and 0.5.

A discussion of the probable range of the cross-section parameter β is presented in appendix C, where it is shown that the most probable value of β lies within the range $0.01 \leq \beta \leq 100$.

Because so little is known about the quantities comprising γ, its probable magnitude cannot be estimated. No recourse exists, therefore, but to determine γ by equating F_{meta} to F_{exp} at one point. The experimental point $x = 0.805$ was arbitrarily chosen.

In the calculations to follow, the values of Ω_x, Ω_0, R_x/R_0, n_{ex}/e_0, and v_x/v_0 used were the raw experimental values presented in figures 6 and 9 to 11, respectively. To eliminate division-by-zero problems in the computer program written to calculate

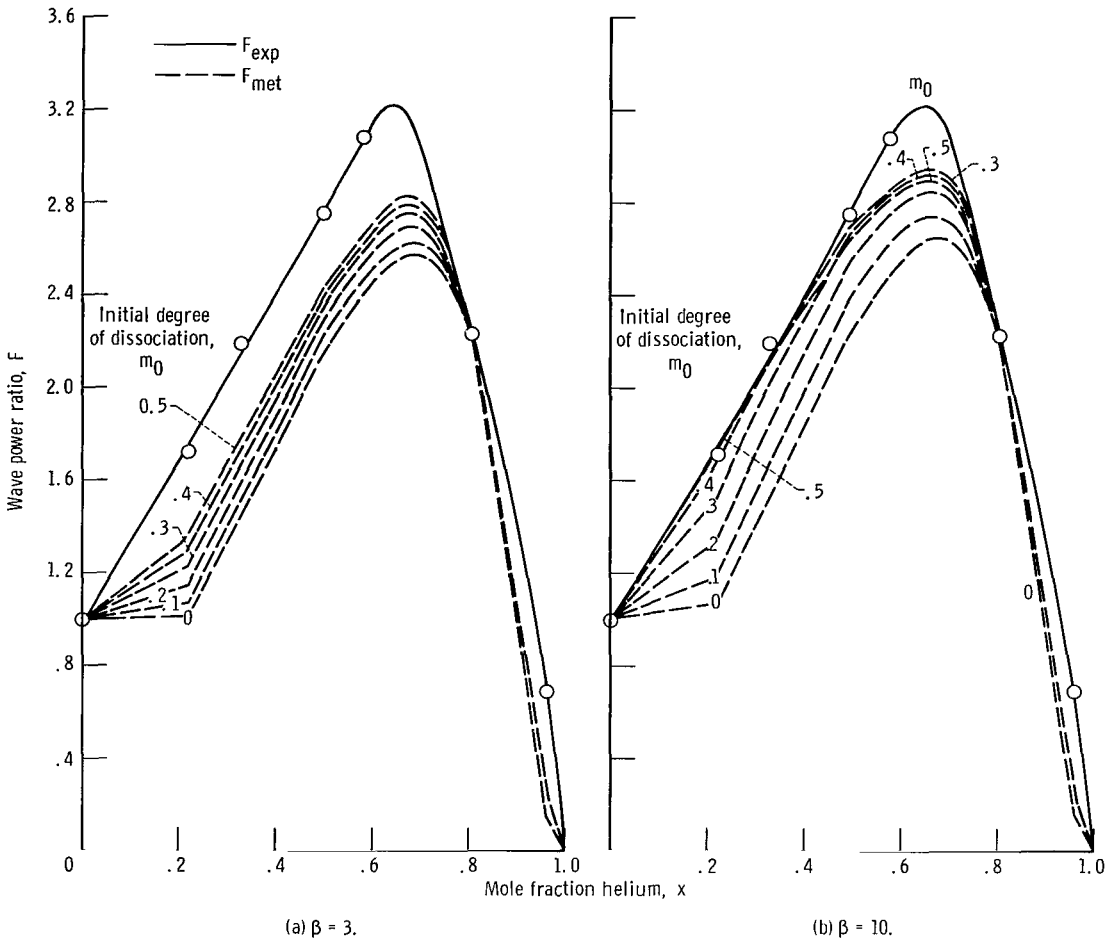

(a) $\beta = 3$. (b) $\beta = 10$.

Figure 12. - Comparison of calculated and experimental wave power ratios for various values of m_0 and β.

F_{met}, the condition $m_0 = 0$ was approximated by setting $m_0 = 1 \times 10^{-6}$. Figure 12(a) portrays the results of setting $\beta = 3$, deriving γ by equating F_{met} to F_{exp} at the $x = 0.805$ point, and letting m_0 take the values 0, 0.01, . . ., 0.5 to yield the family of curves shown. For this value of β, F_{met} does not approach F_{exp} except at the match point. This is true for all smaller values of β as well.

Figures 12(b) to (d) demonstrate the effect of increasing β to 10, 30, and 100, respectively. As β is increased, concordance of F_{met} and F_{exp} occurs at continuously lower values of m_0, F_{exp} being close to the estimated value for the plasma when β is in excess of 30.

As different values of the constants m_0 and β are inserted into equations (39) and (40), different values of the constant γ are also required to equate F_{met} to F_{exp} at $x = 0.805$. These values of γ are reported in figure 13. There is marked on each curve the γ, m_0 pair which yields best concordance between F_{met} and F_{exp} for the value of β chosen. Thus, the line joining these points is the locus of the β, γ, m_0

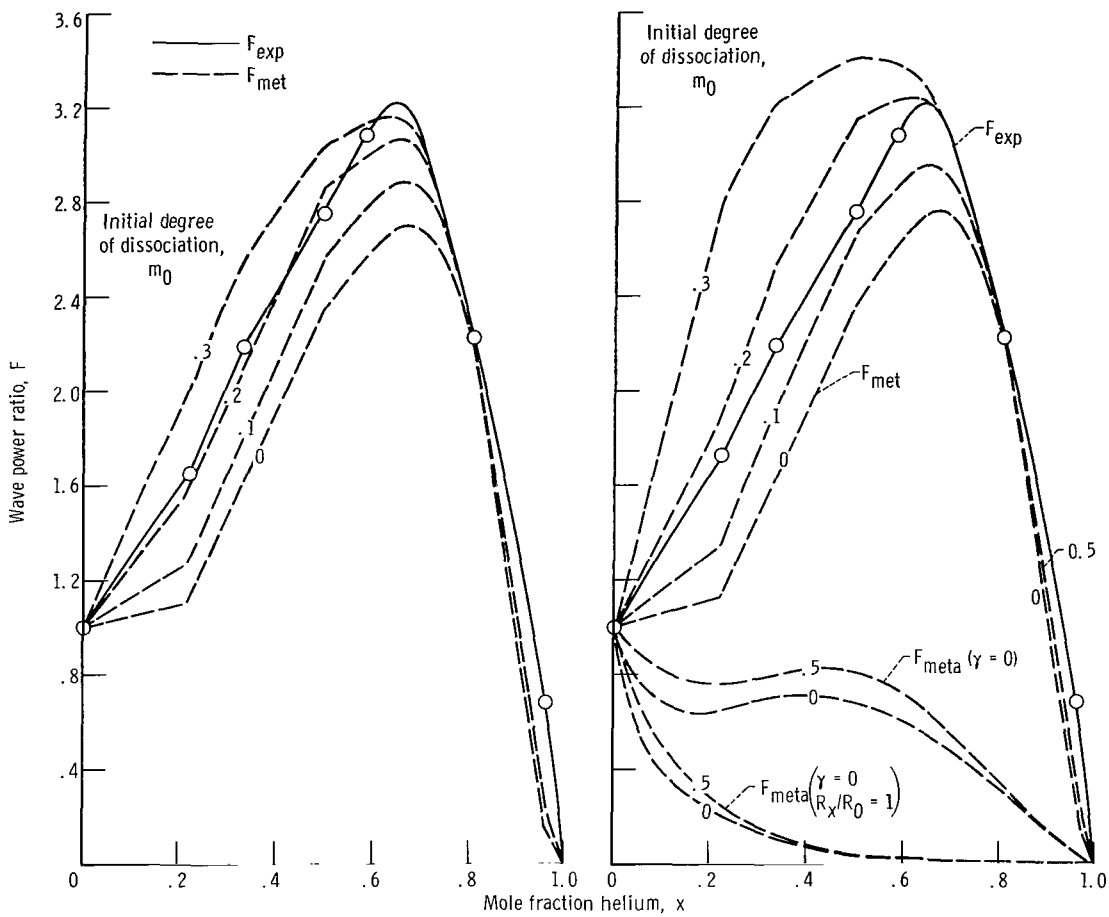

Figure 12. - Concluded.

solution set for the model used to derive F_{met}. This locus does not depend on which experimental point is chosen for the gamma-determining fit, because the best-concordance F_{met} curves agree well with F_{exp} at all points below $x = 0.805$. The agreement at $x = 0.959$ is poor, probably because the model is too simple to adequately treat the case of such small hydrogen concentrations.

In this proposed model, no other effect has been ascribed to helium save the interaction of its metastables with molecular and atomic hydrogen. Hence, the ability of this single assumption to explain the gross features of the experimental power enhancement lends support to the belief that this mechanism plays a major role in the phenomenon observed.

The addition of helium to hydrogen will not result in increased RF power coupling to the plasma in all cases, however. The metastables enhance power addition by providing both increased proton density and increased plasma radius. Thus, it follows that no enhancement of power will occur on addition of helium to a hydrogen plasma whose

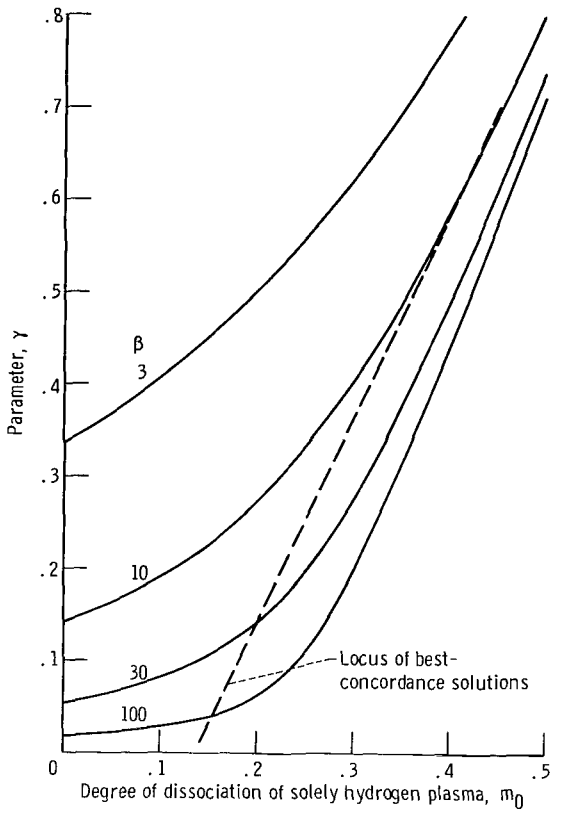

Figure 13. - Relation of γ parameter to m_0 and β.

density is already optimum and whose radius is already the maximum permitted by the discharge container.

That the helium does not act simply as a neutral diluent is readily demonstrable. Were it to do so, the F-behavior of the mixtures would be described by equations (39) and (40) with $\gamma = 0$ and $R_x/R_0 = 1$. Setting $\gamma = 0$ erases only the effect of the proton density enhancement by the helium metastables. This results in the curves labeled $F_{met}(\gamma = 0)$ in figure 15. When, in addition, the increased radius effect produced by the metastables is also erased by setting $R_x/R_0 = 1$, the curves labeled F_{met} ($\gamma = 0$, $R_x/R_0 = 1$) result. This second set of curves clearly disagree with the experimental measurement.

Admittedly, it has not been unequivocally proven that the helium metastables are responsible for the enhanced power absorption in hydrogen-helium mixtures. Admittedly too, the evidence would have been stronger had it been possible independently to arrive at the values of β and γ. Nevertheless, it appears that an explanation for the power enhancement invoking an increased proton concentration through helium metastable interaction is a reasonable explanation of the experimental facts.

SLOT DISCHARGE

As discussed in reference 5, the RF electrostatic shield used in this apparatus was rolled from copper sheet leaving about a 1.8-centimeter slot the full length of the shield. It appeared that a slot of this width permitted some leakage of the E_z component of the electric field of the RF coil to occur, since an enhancement of the radiant plasma intensity is observed in the immediate vicinity of the slot. This so-called slot discharge may be the origin of the small, but finite, difference between the off-resonance plasma power, P_{or} in figure 3, and the base plasma power P_b which is coupled into the plasma. The plasma radius measurements were made on the plasma hemicylinder opposite the slot discharge.

During the preparation of this report, an improved shield design was installed which eliminated the slot discharge and reduced the quantity $P_{or} - P_b$ to zero. Enhancement of power input by the use of hydrogen-helium mixtures occurred nevertheless, indicating that the slot discharge played no dominant role in the enhancement process.

CONCLUDING REMARKS

The ability to couple radio frequency power into a hydrogen plasma is dependent upon many parameters, two of which are proton density and plasma radius. In studying the effect of support gas composition on these two parameters, it was noted that

1. The admixture of helium to the hydrogen plasma atmosphere permitted more power to be coupled into the proton-cyclotron wave. The helium mole fraction of the optimum gas composition was 0.65, for which the wave power input was 3.2 times as great as that for hydrogen alone.

2. An almost linear increase in plasma radius with mole fraction helium x was noted over the range $0 < x < 0.7$, with the radius being observed to maximize near $x = 0.8$.

3. The assumption is made that helium atoms in metastable states enhance the proton density in the plasma by collisions of the second kind with hydrogen atoms and molecules. On this basis, the dependence of the power enhancement on helium content was calculated, and it was found that this mechanism could account for the enhancement experimentally observed.

Lewis Research Center,
National Aeronautics and Space Administration,
Cleveland, Ohio, August 11, 1967,
129-01-05-09-22.

APPENDIX A

SYMBOLS

(The rationalized MKS system of units is used throughout unless otherwise noted.)

A	mass number of ion being resonated, in amu
B	magnetic flux density
B_z	component of magnetic flux density along the z-axis
E	dc potential drop driving the primary beam
e	charge of electron
e*	excitation by electrons
F_{exp}	experimental wave power ratio using experimental power values
F_{met}	calculated wave power ratio based on metastable interaction mechanism defined by equation (15)
I_1, K_1	Bessel functions in the notation of Watson (ref. 9)
I(r)	radial intensity distribution of the plasma
I(Y)	ionization potential of species Y
K	loss rate constant (see reactions of table I)
k	wave number, equal to $2\pi/\lambda$
L_{fs}	ratio of the inductance of the fundamental component of the coil current to the total inductance of the coil system
ℓ	coil length
M	mode number of the plasma oscillation
m	degree of dissociation, defined by equation (24a)
m_p	mass of proton
N	total number of indicated species in the plasma volume
n	proton density, when species is unidentified
$n(\xi)$	number density of species
P	transmitter output power
P_b	no-plasma base power

P_{Or} off-resonant plasma power

P_r transmitter output power at resonance

P_w plasma wave power

Q the ratio of inductive reactance of coil to its resistance

R plasma radius

$\bar{R}$ defined by equation (43)

R_c coil radius

t defined by equation (25)

U defined by equation (2)

V defined by equation (3)

V_m energy of the helium 2^3S metastable state

v closure velocity of electrons with plasma species

w closure velocity of helium metastables with plasma species

x mole fraction helium

Z charge number of ion in ion cyclotron wave

α defined by equation (28a)

β defined by equation (36a)

Δ defined by equation (14)

ξ defined by equation (36b)

$\delta(kR)$ defined by equation (7)

γ defined by equation (28b)

λ wavelength of propagated wave

Ω ratio of coil driving frequency to ion cyclotron frequency

ω transmitter frequency, 41×10^6 rad per sec

σ reaction cross section

ξ dummy argument

Subscripts:

ci ion cyclotron

e electron

j dummy, designating any member of the class under consideration

m metastable state

x the gas mixture whole mole fraction helium is x

0 the gas mixture whose mole fraction helium is 0, that is, pure hydrogen

Superscripts:

* excitation by electrons

m atom in metastable electronic state

o atom in ground electronic state

0 feed gas

APPENDIX B

EVALUATION OF Δ

If the definition of $\delta(kR)$, given by

$$\delta(kR) = \frac{2}{k^2R^2} \frac{I_1(kR)}{K_1(kR)} \tag{7}$$

is substituted into the definition of Δ, given by

$$\Delta = \frac{\delta(k_xR_x)/\delta(k_xR_c)}{\delta(k_0R_0)/\delta(k_0R_c)} \tag{14}$$

then

$$\Delta = \left(\frac{R_0}{R_x}\right)^2 \frac{I_1(k_xR_x)I_1(k_0R_c)}{I_1(k_0R_0)I_1(k_xR_c)} \frac{K_1(k_0R_0)K_1(k_xR_c)}{K_1(k_xR_x)K_1(k_0R_c)} \tag{B1}$$

To evaluate the Bessel functions, absolute numerical values must be obtained for the arguments. From the dispersion relation (eq. (4)),

$$\frac{1}{\lambda} = \Omega\left[\frac{n}{2.03\times10^{18}(1 - \Omega^2)}\right]^{1/2} \tag{B2}$$

so that, from the definition $k = 2\pi/\lambda$,

$$k_x = 2\pi\Omega_x\left[\frac{n_x}{2.03\times10^{18}\left(1 - \Omega_x^2\right)}\right]^{1/2} \tag{B3}$$

Absolute values of n_x are not known, but n_0 is known to be near 1×10^{17} per cubic meter. Hence, if the relation between n_x and n_0 is known, we may write

$$k_x = 4.41\times10^{-9}\, n_0^{1/2}\left[\frac{(n_x/n_0)\Omega_x^2}{1 - \Omega_x^2}\right]^{1/2} \tag{B4}$$

TABLE II. - VALUES OF Δ

Mole fraction helium, x	Wave number, k_x, m^{-1}	Δ
0	4.386	1.000
.220	4.344	1.003
.328	4.275	.997
.495	3.639	1.022
.580	3.521	1.035
.805	2.843	1.051
.959	1.223	1.126

where n_x/n_0 will be taken to be given by equation (31).

Absolute values for the proton plasma radius must also be specified, which are most conveniently written in the form

$$R_x = R_0(R_x/R_0) \tag{B5}$$

R_x/R_0 being given in figure 9. No alternative exists but to use $\bar{R}$ for the proton plasma radius, so that $R_0 = 1.03$ centimeters. The mean coil radius R_c is 7.3 centimeters.

All quantities being now specified, $\Delta = \Delta(x)$ may be calculated. The results are given in table II, which show that $\Delta(x)$ does not deviate appreciably from unity. However, were the x-dependence of Δ taken into account, a closer fit of F_{met} to F_{exp} would result. Thus, the approximation $\Delta = 1$ does not introduce any degree of conformity between theory and experiment.

APPENDIX C

PROBABLE HYDROGEN PLASMA REACTIONS

Electron Impact Processes

If possessed of sufficient energy, electrons colliding with hydrogen molecules may generate a variety of reactions. Consider the partial energy level diagram of the hydrogen molecule (ref. 10) presented in figure 14. The spectroscopic notation used is defined in reference 11. Electron impact excitation may produce any of the excited states shown. The net effect of exciting these states are tabulated in table III.

The first excited state (in order of increasing energy and decreasing cross-section) is the $1s\sigma\ 2p\sigma\ {}^3\Sigma_u^+$ state, which is dissociative. Thus, any molecule excited to this state will immediately dissociate into two ground state atoms. Furthermore, the excitation of the molecule to any of the bonding triplet states will ultimately result in dissociation also, because all ${}^3\Sigma_g$ and ${}^3\Pi_g$ states produced can radiate to the dissociative ${}^3\Sigma_u$, and all bonding ${}^3\Sigma_u$ and ${}^3\Pi_u$ states can radiatively cascade through the $1s\sigma 2s\sigma {}^3\Sigma_g^+$ state to the dissociative ${}^3\Sigma_u^+$. Thus, all triplet state excitation of

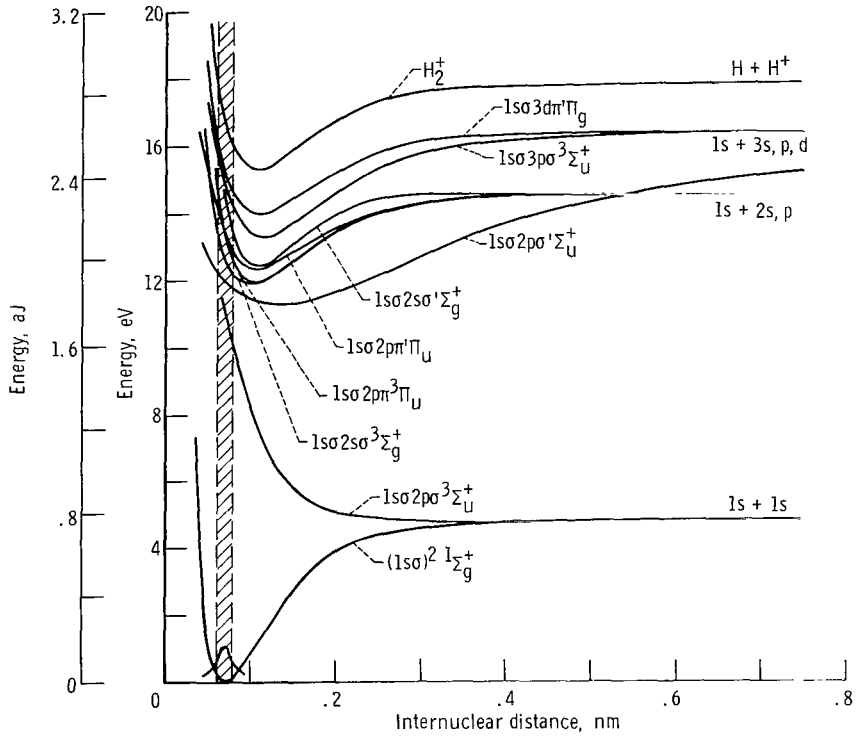

Figure 14. - Potential energy curves for some typical states of hydrogen molecule.

TABLE III. - HYDROGEN PLASMA REACTIONS

Reaction number	Reaction	Cross section
1e	$H_2 \xrightarrow{e^*} H_2^*(1s\sigma 2s\sigma\, {}^3\Sigma_u^+) \xrightarrow{\text{Spontaneous dissociation}} 2H$ $H_2 \xrightarrow{e^*} H_2^*(\text{bound triplets}) \xrightarrow{-h\nu} H_2^*(1s\sigma 2s\sigma\, {}^3\Sigma_u^+)$	σ_1
1m	$H_2 \xrightarrow{He^m} H_2^*(1s\sigma 2s\sigma\, {}^3\Sigma_u^+) \xrightarrow{\text{Spontaneous dissociation}} 2H$	σ_2
2e	$H_2 \xrightarrow{e^*} H_2^+ + e$	σ_6
3e	$H_2 \xrightarrow{e^*} H + H^+ + e$	σ_7
4e	$H \xrightarrow{e^*} H^+ + e$	σ_3
4m	$H \xrightarrow{He^m} H^+ + e$	σ_4

molecular hydrogen will ultimately produce a net dissociative reaction. In table III, the short hand description of this process is designated as reaction 1e.

Electron excitation of ground state molecules to excited singlet states can occur too, but these can all return radiatively to the ground state either directly or through a cascade path. Thus, excitation of singlet states results only in radiative energy losses, but no dissociation. There being no useful result, the singlet state excitation process is not depicted in table III.

The preceding discussions are predicated on the premise that electrons are colliding with hydrogen molecules not only in their ground electronic state, but in their ground vibrational state as well. Under conditions of adiabatic excitation, that is, where the excitation occurs so quickly that the molecular nuclei are unable to move much in the elapsed time, the internuclear separation of the excited state produced will be closely the same as that of the target molecule at the instant that excitation occurred. If attention is now directed to any of the excited state Morse curves in figure 14 and especially to the ground state of the hydrogen molecular ion (H_2^+), it may be observed that excitation at sufficiently small internuclear separation could yield excited states with sufficient vibrational energy to be dissociative. However, as a result of a program undertaken to calculate the electron impact cross sections of the excited states of molecular hydrogen (ref. 11), it was found that the fraction of ground state molecules having internuclear separations small enough to produce dissociative excited states was negligible.

Applying these considerations to ionization of the hydrogen molecule leads directly to the conclusion that the products of the ionizing electron impacts will be almost wholly

H_2^+, with very little H and H^+, the products of a dissociative ionization. Thus reaction 2e of table III should have a high cross section and will thus be important, whereas reaction 3e should have a low cross section and thus be unimportant. Indeed, the experiments of Tate and Smith and of Newhall, as reported by Goodyear and Von Engel (ref. 12), bear out these conclusions.

Having surveyed the possible reactions of molecular excitation and failing to find a proton source among them, it follows that the proton source must be ionization of the atomic hydrogen produced by reaction 1e. Thus, reaction 4e of table III is assigned as the proton source in a hydrogen plasma, not only by elimination, but also because it is a high cross section reaction, to which reference 11 testifies.

Helium Metastable Interactions

The helium 2^3S_1 and 2^1S_0 metastable states have energies of 19.8 and 20.6 eV (3.17 and 3.30 aJ), respectively. Thus, more than enough energy is available to permit these metastables to dissociate hydrogen molecules or ionize hydrogen atoms on collision with them. Considering the second possibility first, examine the reaction

$$He^m(2^3S) + H \rightarrow He^o + H^+ + e + 6.3\ eV \qquad (C1)$$

and enter it as reaction 4m in table III. The cross section for this reaction is not known. However, Penning reactions such as this have been known for many years, and it will be instructive to inquire into the magnitude of the cross sections of those reactions which have been studied. For the reaction

$$He^m(2^3S) + x \rightarrow He^o + Y^+ + e + \text{energy excess} \qquad (C2)$$

the energy excess is given by

$$\text{Energy excess} = V_m - I(Y) \qquad (C3)$$

where V_m is the potential energy of the metastable state and I(Y) is the ionization potential of the species Y. Figure 15 is a plot of the cross section for the He^m - Y reaction against the energy excess of the reaction, the data being taken from references 13 and 14. One observes that the cross section for the reaction appears to increase linearly with energy excess. Since there is no reason to expect that atomic hydrogen should behave any differently from argon, krypton, or xenon as a Penning gas, then the cross section of reaction 4m might be predicted to be about 10×10^{-16}

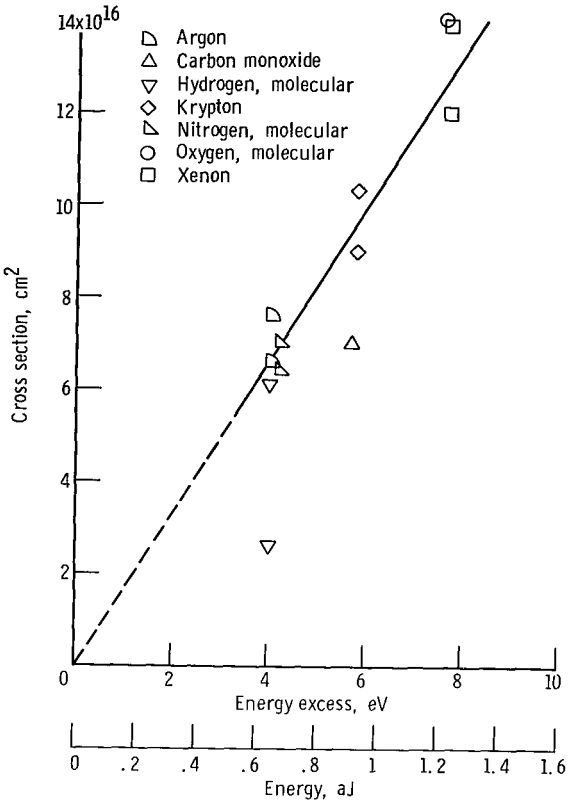

Figure 15. - Cross-sections of various gases for Penning ionization by helium triplet metastables.

square centimeter since its energy excess is 6.3 eV (1.01 aJ). This is a sizable cross section and, if true, would support the assumption that Penning effect ionization of atomic hydrogen is a significant source of protons in our plasma.

The Penning ionization is, of course, simply a specific case of a general class of reactions, namely, collisions of the second kind, where the potential energy of the incident particle is transformed in significant measure to potential energy of the target particle, with the excess providing kinetic energy of separation of the reaction products. Thus, when a metastable collides with a molecule, it is possible that electronic excitation of the molecule may occur, not only into the ionization continuum, but also into an excited repulsive state from which dissociation will result. Groth and Oldenberg (ref. 15) propose this mechanism to explain the enhancement of nitrogen dissociation by excited krypton states.

Furthermore, Beutler and Eisenschimmel (ref. 16) showed that neon metastables produced dissociation of molecular hydrogen. Thus, for the interaction of helium metastables with molecular hydrogen the analog to reaction 1e is added to table III as reaction 1m. From figure 12(d), the excitation potential of the repulsive $^3\Sigma_u^+$ state at 0.074 nanometer is about 11 eV.

Unfortunately, no quantitative data is available for dissociative reactions between metastables and molecules.

Estimation of β

Fortunately, it is not necessary to have numerical values for the cross sections of table III. What is necessary is only to estimate the value of β, which is defined by equation (36a) to be

$$\beta \equiv \frac{\sigma_2}{\sigma_4}\frac{\sigma_3}{\sigma_1} \tag{C4}$$

Thus, β is the product of two ratios. To evaluate it, consider first the ratio σ_2/σ_4, which involves the cross section for the reactions 1m and 4m of table III. The Penning ionization reaction (shown as eq. (C1)) involves basically the formation of a collision complex between two particles which subsequently decomposes into three particles, namely, a helium atom, a proton, and an electron. But reaction 1m involves also the formation of a collision complex between two particles which subsequently decomposes into three particles, namely, a helium atom and two hydrogen atoms. Thus, both reactions involve the transformation of the potential energy of the metastable state into potential energy required to break bonds in the target species plus kinetic energy to separate the product species. In this light, reactions 1m and 4m are similar, whereupon the assumption that σ_2 is within an order of magnitude of σ_4 seems valid. Thus,

$$0.1 \leq \sigma_2/\sigma_4 \leq 10 \tag{C5}$$

Regarding the ratio σ_3/σ_1, data for both these cross sections as a function of monoenergetic electron energy exist in the literature (refs. 17 and 18). After these data have been transformed to yield the cross sections as a function of Maxwell averaged electron energy, the electron energy dependence of the ratio σ_3/σ_1 may be found. The ratio is 0.01 at 1 eV (0.16 aJ) and increases monotonically to 8 at 50 eV (8 aJ). Because this is the energy range that has been measured in the plasma by probe and spectrometric techniques (ref. 6), it is assumed that

$$0.01 \leq \sigma_3/\sigma_1 \leq 8 \tag{C6}$$

Thus, we shall expect to find β within the range

$$0.001 \leq \beta \leq 80 \tag{C7}$$

REFERENCES

1. Stix, T. H.; and Palladino, R. W.: Experiments on Ion Cyclotron Resonance. Phys. Fluids, vol. 1, no. 5, Sept.-Oct. 1958, pp. 446-451.

2. Hooke, W. M.; Tenney, F. H.; Brennan, M. H.; Hill, H. M., Jr.; and Stix, T. H.: Experiments on Ion Cyclotron Waves. Phys. Fluids, vol. 4, no. 9, Sept. 1961, pp. 1131-1141.

3. Woollett, Richard R.: Frequency Ranges for Existence of Waves in a Cold, Collisionless Hydrogen Plasma. NASA TN D-2273, 1964.

4. Swett, Clyde C.; and Krawec, Roman: Preliminary Observations of RF Power Transfer to a Hydrogen Plasma at Frequencies near the Ion Cyclotron Frequency. Proceedings of the Third Symposium on Engineering Aspects of Magnetohydrodynamics. Norman W. Mather and George W. Sutton, eds., Gordon and Breach Science Publishers, Inc., 1964, pp. 599-614.

5. Swett, C. C.; Krawec, R.; Prok, G. M.; and Hettel, H. J.: Experiments on Ion-Cyclotron-Wave Generation Using An Electrostatically-Shielded RF Coil. Paper presented at the American Physical Society Meeting, Washington, D. C. Apr. 26-29, 1965 (Also available as NASA TM X-52091, 1965).

6. Krawec, Roman; Prok, George M.; and Swett, Clyde C.: Evaluation of Two Direct-Current Methods of Plasma Production for Use in Magnetic Mirror Experiments. NASA TN D-2862, 1965.

7. Stix, Thomas H.: Generation and Thermalization of Plasma Waves. Phys. Fluids, vol. 1, no. 4, July-Aug. 1958, pp. 308-317.

8. Bockasten, Kjell: Transformation of Observed Radiances into Radial Distribution of the Emission of a Plasma. J. Opt. Soc. Am., vol. 51, no. 9, Sept. 1961, pp. 943-947.

9. Watson, G. N.: A Treatise on the Theory of Bessel Functions. Second ed., The Macmillan Co., 1944.

10. Kauzmann, Walter: Quantum Chemistry. Academic Press, Inc., 1957 (Second Printing, 1959), p. 397.

11. Prok, G. M.; Monnin, C. F.; and Hettel, H. J.: Estimation of Electron Impact Excitation Cross Sections of Molecular Hydrogen. NASA TN D-4004, 1967.

12. Goodyear, C. C.; and Von Engel, A.: Atomic Ion Production in Radio-Frequency Ion Sources. Proceedings of the Fifth International Conference on Ionization Phenomena in Gases. H. Maecher, ed., North Holland Publ. Co., 1962, pp. 203-213.

13. Sholette, W. P.; and Muschlitz, E. E., Jr.: Ionizing Collisions of Metastable Helium Atoms in Gases. J. Chem. Phys., vol. 36, no. 12, June 15, 1962, pp. 3368-3373.

14. Benton, E. E.; Ferguson, E. E.; Matsen, F. A.; and Robertson, W. W.: Cross Sections for the De-Excitation of Helium Metastable Atoms by Collisions with Atoms. Phys. Rev., vol. 128, no. 1, Oct. 1, 1962, pp. 206-209.

15. Groth, W. E.; and Oldenberg, O.: Dissociation by Impacts of the Second Kind. J. Chem. Phys., vol. 23, no. 4, Apr. 1955, pp. 729-731.

16. Mitchell, Allan C. G.; and Zemansky, Mark W.: Resonance Radiation and Excited Atoms. Cambridge University Press, 1934 (Second Printing, 1961), p. 86.

17. Engelhardt, A. G.; and Phelps, A. V.: Elastic and Inelastic Collision Cross Sections in Hydrogen and Deuterium from Transport Coefficients. Phys. Rev., vol. 131, no. 5, Sept. 1, 1963, pp. 2115-2128.

18. Kieffer, L. J.; and Dunn, Gordon H.: Electron Impact Ionization Cross-Section Data for Atoms, Atomic Ions, and Diatomic Molecules: I. Experimental Data. Rev. Mod. Phys., vol. 38, no. 1, Jan. 1966, pp. 1-35.

NASA-Langley, 1968 —— 25 E-3402